Coupled Lake-Atmosphere-Land Physics Uncertainties in a Great Lakes Regional Climate Model

William J. Pringle[1], Chenfu Huang[2], Pengfei Xue[1,2], Jiali Wang[1], Khachik Sargsyan[3], Miraj B. Kayastha[2], TC Chakraborty[4], Zhao Yang[4], Yun Qian[4], Robert D. Hetland[4]

[1]Environmental Science Division, Argonne National Laboratory, Lemont, IL, USA
[2]Department of Civil, Environmental and Geospatial Engineering, Michigan Technological University, Houghton, MI, USA
[3]Sandia National Laboratories, Livermore, California, USA
[4]Pacific Northwest National Laboratory, Richland, WA, USA

Key Points:

- Atmospheric physics parameterizations and their interactions with lake physics are dominant drivers of surface temperature uncertainty.
- Surface temperatures are more uncertain over the deeper northern lakes and forested northern land areas than in the south.
- Uncertainty increases on/over the lakes during rapid spring warming and over the southwest land area during multiday temperature declines.

Corresponding author: William Pringle, `wpringle@anl.gov`

Abstract

This study develops a surrogate-based method to assess the uncertainty within a convective permitting integrated modeling system of the Great Lakes region, arising from interacting physics parameterizations across the lake, atmosphere, and land surface. Perturbed physics ensembles of the model during the 2018 summer are used to train a neural network surrogate model to predict lake surface temperature (LST) and near-surface air temperature (T2m). Average physics uncertainties are determined to be 1.5°C for LST and T2m over land, and 1.9°C for T2m over lake, but these have significant spatiotemporal variations. We find that atmospheric physics parameterizations are the dominant sources of uncertainty for both LST and T2m, and there is a substantial atmosphere-lake physics interaction component. LST and T2m over the lake are more uncertain in the deeper northern lakes, particularly during the rapid warming phase that occurs in late spring/early summer. The LST uncertainty increases with sensitivity to the lake model's surface wind stress scheme. T2m over land is more uncertain over forested areas in the north, where it is most sensitive to the land surface model, than the more agricultural land in the south, where it is most sensitive to the atmospheric planetary boundary and surface layer scheme. Uncertainty also increases in the southwest during multiday temperature declines with higher sensitivity to the land surface model. Last, we show that the deduced physics uncertainty of T2m is statistically smaller than a regional warming perturbation exceeding 0.5°C.

Plain Language Summary

Regional climate models couple together lake, atmosphere, and land surface components, each containing several simplifications of complex small-scale physics, known as parameterizations. In this study, we explore the uncertainty arising from the choice of interacting parameterizations and associated parameters across coupled lake-atmosphere-land components of a Great Lakes regional climate model. To do this, we train a machine learning surrogate model on the climate model outputs of lake and air surface temperatures during the 2018 summer. The surrogate model is then rapidly queried thousands of times to find the uncertainty range and which physics parameterizations contribute to it. We find that atmospheric physics parameterizations are the dominant sources of uncertainty and that there is a substantial atmosphere-lake physics interaction component. The surface temperatures are more uncertain over the deeper northern lakes and forested northern land areas than over the shallower lakes and more agricultural land in the south. Uncertainty increases on and over the lakes during a time of rapid warming in the late spring/early summer, and over the southwest land area during periods where the temperature drops over multiple days. We also show that the physics uncertainty of surface temperature is much smaller than mid-21st century regional warming projections.

1 Introduction

Uncertainty about the physical processes in the atmosphere, water bodies, and the land surface can contribute to biases and large spread in weather and climate models (Bellprat et al., 2012b; Ricciuto et al., 2018; Zanna et al., 2019; Eidhammer et al., 2024). This is most often attributable to unresolved physics requiring parameterizations that, while often based on theory, are necessarily simplifications requiring several assumptions and free empirical parameters. To appropriately deal with the inevitable presence of this epistemic uncertainty, the weather and climate modeling fields have employed the use of Perturbed Physics/Parameter Ensembles (PPE; Bellprat, Kotlarski, Lüthi, & Schär, 2012a; Eidhammer et al., 2024). Several PPE-based studies have investigated processes in the atmosphere (Bellprat et al., 2012a; Qian et al., 2015, 2018, 2024), land surface processes

(Ricciuto et al., 2018; Xu et al., 2022), and oceans (Huber & Zanna, 2017). Land-atmosphere interactions were investigated in C. Wang et al. (2021).

Prior PPE studies have rarely focused on complex coastal systems, where interactions between the atmosphere, land and water bodies can collectively modulate these uncertainties. One region where these interactions are important and not well-assessed by the climate modeling communities is the Great Lakes of North America (Sharma et al., 2018; J. Wang et al., 2022), the world's largest surface freshwater system. Many climate models have used a simplified representation of the lake surface, and thus may not adequately capture the impact of the lakes on the regional climate (Briley et al., 2021). However, several recent studies have now incorporated coupled three-dimensional (3-D) hydrodynamic processes of the lakes into regional climate models focused on the Great Lakes region (GLR; Xue et al., 2017; Sun, Liang, & Xia, 2020; Xue et al., 2022; Kayastha et al., 2023). To date, investigation of physics parameterizations in GLR regional climate models has been limited to ad-hoc performance evaluation experiments without the 3-D lake (Notaro et al., 2021), and without a formal PPE analysis.

One of the reasons for the lack of in-depth analysis of parameterizations of unresolved physics across the lakes, atmosphere, and land is that running coupled models with perturbations across all model components is computationally costly. To mitigate this issue, PPE studies have adopted the use of surrogate models (Ricciuto et al., 2018). Surrogate models are extremely inexpensive to query, often based on linear models or polynomials (Qian et al., 2018; Bellprat et al., 2012b; Ricciuto et al., 2018), so that the entire uncertainty space can be explored. However, this requires the generation of an adequate surrogate model in the first place. Further, we are typically interested in how the uncertainties and interactions vary across space and time, hence we need a way to deal with the large dimensionality of the model.

This paper focuses on addressing the problem of assessing physics uncertainties across a complex atmosphere-land-lake system. We develop a surrogate model-based framework that is, in principle, generalizable to all regional climate models and apply it to simulations of the GLR with a newly developed coupled modeling system (Kayastha et al., 2023). We investigate the sensitivity of (near-)surface temperature, a critical component of the surface energy budget, to variations in parameterizations/parameters, and quantify the contribution of each parameterization/parameter to this uncertainty. The variation of this physics uncertainty across space and time and the importance of the coupled effects is highlighted. Implications of the uncertainty on climate projections of surface temperature in the GLR are also discussed.

2 Methods and Data

2.1 Model Description and Experimental Design

2.1.1 Coupled Lake-Atmosphere Model Configuration

We use a two-way coupled atmosphere and 3-D hydrodynamic lake modeling setup developed by Kayastha et al. (2023) for our PPE analysis. The atmosphere component is the Weather Research and Forecasting (WRF) model v4.2.2 (Skamarock et al., 2021) with the Advanced Research WRF (ARW) dynamic core (Skamarock & Klemp, 2008). The hydrodynamic lake component is based off of the Finite Volume Community Ocean Model (FVCOM; Chen, Liu, & Beardsley, 2003) v4.1 (see more descriptions below). The coupled atmosphere-lake model domain is centered at 45.5°N and 85.0°W and has dimensions of 543×484 grid points in the west-east and south-north. Grid spacing is 4 km, covering the GLR (Figure 1). There are 50 stretched vertical levels topped at 50 hPa. The initial and boundary conditions are from 3-hourly 0.25° European Centre for Medium-Range Weather Forecasts atmospheric reanalysis of the global climate, version 5 (ERA5; Hersbach et al., 2020).
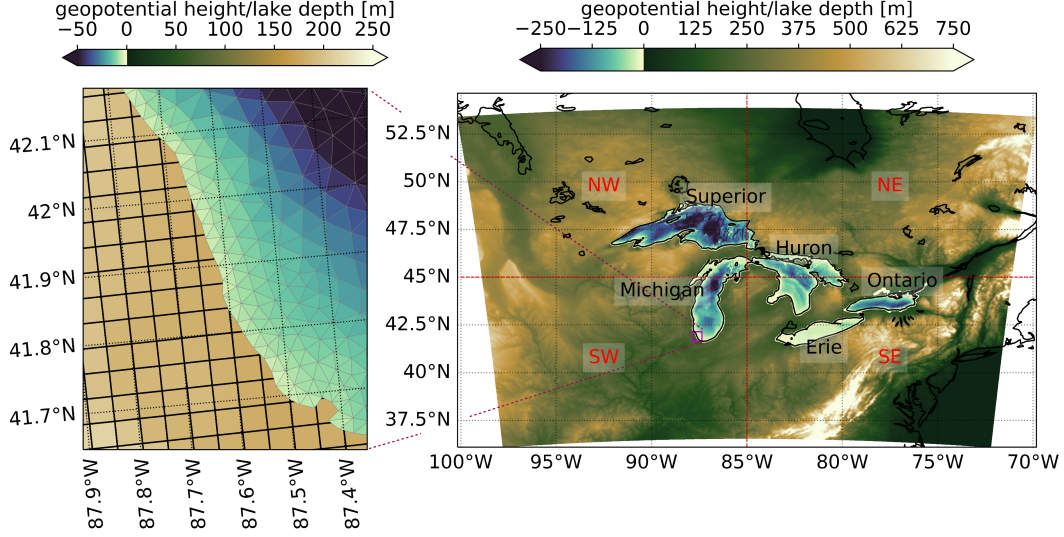
Figure 1. Computational domain of the WRF-FVCOM model with zoom-in view of grid sizes near the Chicago coastline. Shading shows the geopotential height in the WRF atmosphere model and bathymetric depths in the FVCOM lake model. Labels denote lake names and land area quadrants.

Three commonly used physics options each for cloud microphysics (MP), longwave and shortwave radiation (LW+SW RA), and planetary boundary layer and surface layer (PBL+SFC), and two land surface models (LSM) are used in this study, as summarized in Table 1. The default configuration from our previous studies (Kayastha et al., 2023; J. Wang et al., 2022) is indicated in the table. In this study, we modified the source codes of the SFC scheme in WRF so that each SFC scheme can use one of any three chosen parameterizations of surface roughness length over water ($z0_w$): constant Charnock coefficient of 0.0185, the Coupled Ocean–Atmosphere Response Experiment (COARE) 3.5 algorithm (Edson et al., 2013), or the depth-dependent over shallow waters (<100 m) scheme (Jiménez & Dudhia, 2018). Our hypothesis is that the depth-dependent scheme should improve surface variables over the Great Lakes as a large portion is <100 m deep (Figure 1).

The hydrodynamic lake component is based off of the Finite Volume Community Ocean Model (FVCOM; Chen et al., 2003) v4.1. Horizontal resolution on an unstructured triangular mesh varies from 2-4 km offshore to 1-2 km along the coasts (Figure 1), and the model has 40 vertical sigma layers (Kayastha et al., 2023). The model is initialized from a quiescent state in the winter when the lakes are unstratified with an initial uniform lake temperature of 2°C. As in Kayastha et al. (2023), FVCOM is run simultaneously with WRF, including a two-way information exchange between them at 1-hr intervals using the OASIS3-MCT coupler (Craig et al., 2017). Here, the LST and ice cover are dynamically calculated by FVCOM and are provided to WRF as overlake surface boundary conditions. In turn, the atmospheric forcings required by FVCOM are dynamically calculated and provided by WRF (see a more detailed discussion in Kayastha et al., 2023).

FVCOM parameterization options and parameters are summarized in Table 1. Vertical mixing (VM) is modeled with either the Mellor-Yamada Level 2.5 (MY-2.5) closure (Mellor & Yamada, 1982) or the General Ocean Turbulence Model (GOTM) implementation of the k-ϵ closure (Stips et al., 2002). We use the Large and Pond (1981) or Andreas et al. (2012) bulk wind stress (WS) parameterization to impart momentum from the at-

145 mosphere into the lake at the surface. Lastly, we vary two uncertain parameters: the tur-
146 bulent Prandtl number (Pr_t) and R: the fraction of the downward shortwave flux asso-
147 ciated with the longer wavelength irradiance. We vary Pr_t from 0.1 to 1 and R from 0.74
148 to 0.78, the latter representing a range from relatively clear Type IA water to lower clar-
149 ity Type III water (Paulson & Simpson, 1977). We also assign values to the two other
150 variables in the shortwave radiation absorption formulation dependent on R: the atten-
151 uation depth for the longer wavelength component of shortwave irradiance, $\zeta_1 = 1.7+$
152 $0.3\alpha_R$ and the attenuation depth for shorter wavelength component of shortwave irra-

Table 1. Uncertain physics parameterizations and parameters in the coupled WRF-FVCOM model. Detailed descriptions of WRF parameterizations can be found in Skamarock et al. (2021). See text for description of FVCOM parameterizations and parameters.

Parameter(ization)	Definition	Options	Priors
PBL+SFC	WRF planetary boundary layer and surface scheme	YSU + MM5$_{rev}$* MYJ + MOJ MYNN-2.5 + MYNN	$\mathcal{U}_d[1,3]$
MP	WRF cloud microphysics scheme	Morrison Thompson* WSM6	$\mathcal{U}_d[1,3]$
LW+SW Rad	WRF longwave and shortwave radiation scheme	RRTM + CAM3 RRTMG + RRTMG* Goddard + Goddard	$\mathcal{U}_d[1,3]$
z0$_w$	WRF surface roughness length over water scheme	COARE 3.5 Charnock = 0.0185* Depth-dependent	$\mathcal{U}_d[1,3]$
LSM	WRF land surface model	Noah* Noah-MP	$\mathcal{U}_d[1,2]$
VM	FVCOM vertical mixing scheme	MY-2.5* GOTM k-ϵ	$\mathcal{U}_d[1,2]$
WS	FVCOM bulk wind stress parameterization	Large and Pond (1981)* Andreas et al. (2012)	$\mathcal{U}_d[1,2]$
Pr_t	FVCOM turbulent Prandtl number	value from 0.1 to 1*	$\mathcal{U}[0.1,1]$
R	FVCOM shortwave radiation absorption fraction	value from 0.74 to 0.78*	$\mathcal{U}[0.74,0.78]$

*Indicates settings of the default setup from Kayastha et al. (2023)
YSU: Yonsei University PBL, MYJ: Mellor-Yamada-Janjic PBL
MYNN-2.5: Mellor-Yamada-Nakanishi-Niino Level 2.5 PBL
MM5$_{rev}$: revised fifth-generation PSU–NCAR Mesoscale Model SFC
MYJ: Monin-Obukhov-Janjic SFC, MYNN: Mellor-Yamada-Nakanishi-Niino SFC
Morrison: Morrison double-moment 6-class MP, Thompson: Thompson double-moment 6-class MP
WSM6: WRF single-moment 6-class MP, RRTM: Rapid Radiative Transfer Model RAD
RRTMG: Rapid Radiative Transfer Model for General Circulation Models RAD
CAM3: NCAR Community Atmosphere Model 3.0 RAD, Goddard: New NASA Goddard RAD
Noah: Unified Noah LSM, Noah-MP: Noah-multiparameterization LSM
MY-2.5: Mellor-Yamada Level 2.5 VM, GOTM k-ϵ: General Ocean Turbulence Model k-ϵ VM

153 diance, $\zeta_2 = 6 + 9.7\alpha_R$, in which $\alpha_R = (0.74 - R)/0.04$, based on values from Paulson
154 and Simpson (1977); Chen et al. (2011).

2.2 Model Uncertainty Analysis

156 We use a surrogate model framework for the forward uncertainty propagation of
157 the expensive coupled lake-atmosphere-land physics model. In this framework, physics
158 parameterizations and parameters are assigned a statistical distribution (typically uni-
159 form or Gaussian) a priori by the modeler, hereafter termed the "parametric priors" and
160 denoted by $\boldsymbol{\lambda}$. For the physics parameterizations, a discrete uniform distribution is cho-
161 sen, $\mathcal{U}_d[1, N_s]$, where the value of the integer corresponds to a specific scheme in the range
162 from 1 to the number of chosen schemes, N_s. As the order of these integers is unimpor-
163 tant, one hot encoding is used to covert to binary representations before surrogate model
164 training. For the parameters, a continuous uniform distribution, $\mathcal{U}[a, b]$, is chosen to range
165 between deemed plausible values a and b. The parametric priors for the coupled lake-
166 atmosphere-land model are summarized in Table 1.

167 To generate the surrogate model for the uncertainty analysis, a training set is re-
168 quired from samples of the physics model. To form this training set, the joint distribu-
169 tion of the parametric priors must be sampled efficiently, typically using Quasi-Monte
170 Carlo (QMC) or Latin hypercube sampling (Qian et al., 2015). The sampling method
171 used in this study (QMC) is detailed in section 2.3. From this training set, a surrogate
172 model is generated to approximate the quantity of interest (QoI),

$$Z = f(\boldsymbol{\lambda}, \boldsymbol{x}, t) \approx g(\boldsymbol{\lambda}, \boldsymbol{x}, t) \tag{1}$$

173 where Z is the spatiotemporally varying modeled QoI as a function of the parametric
174 priors $\boldsymbol{\lambda}$, and can be approximated by the surrogate model, g. In this study, we use a
175 multilayer perceptron artificial neural network (NN) surrogate model with a Rectified
176 Linear Unit (ReLu) activation function, implemented with *PyTorch* (Paszke et al., 2019).
177 We also implemented a Polynomial Chaos (Sargsyan et al., 2014) surrogate model in the
178 code distributed with this study. However, it did not perform as well as the NN model,
179 so we do not show those results here. This is expected for polynomials, as they are not
180 well-suited to discrete inputs that we use for physics parameterizations, but we included
181 it in the code for potential future use in an analysis with only continuous parameter in-
182 puts (e.g., Ricciuto et al., 2018).

183 Based on the formation of g, a global sensitivity analysis (GSA) and determina-
184 tion of the distribution of the QoI can be performed rapidly through Monte Carlo sam-
185 pling of the surrogate models. Variance-based Sobol sensitivity indices are computed us-
186 ing a GSA sampling scheme from Saltelli (2002). The GSA samples are also used to cal-
187 culate the uncertainty, which we define as the 90% interval, i.e., the range between the
188 5th and 95th percentiles of the distribution.

2.3 Computational Design and Surrogate Model Construction

190 Our simulations target the analysis of 2018 summer season (JJA), with May 2018
191 used as the spinup period (Kayastha et al., 2023). During this period, the lakes go through
192 a rapid spring warming phase due to radiatively driven convection (Austin, 2019) and
193 become strongly stratified with stable lake temperatures for the rest of the season. The
194 warming phase occurs earliest in May-June for the southern shallow lakes (Erie and On-
195 tario) and latest in June-July for the northern deep lakes (Superior, Huron, and Michi-
196 gan). This season thus presents an interesting period of time to investigate the lake-atmosphere
197 coupling and its sensitivity to different forms of physics parameterizations and param-
198 eter quantities. The model performance has been evaluated compared to observations
199 in Kayastha et al. (2023).

An ensemble of simulations is carried out by sampling the $9 (=N_d)$ parametric priors (Table 1) with a QMC low-discrepancy Korobov sequence from *chaospy*. A total of 18 ensemble members $(=N_e)$ for training are requested. This number was chosen because, 1) close to 90% (actually 89.5%) of the distribution of a continuous variable is sampled using the Korobov sequence (W. J. Pringle et al., 2023), and 2) the discrete variables have either 2 or 3 unique values, so 18 samples each parameterization option an equal number of times (6 or 9), which is a requirement of uniform design (Fang et al., 2000), a method akin to the present approach given our assumption of uniformly distributed priors. A small test set of 5 ensemble members $(=N_{et})$ is also produced for validation purposes.

The QoIs chosen for the sensitivity assessment are daily mean 2-m air temperature (T2m) and lake surface temperature (LST). Hourly outputs from the WRF-FVCOM at each available grid point are processed into the daily quantities. Analysis is performed on the full spatiotemporal dataset for each QoI. In total we have $N_t = 92$ days with N_p = 262,812 WRF grid points for T2m and $N_p = 35,749$ FVCOM grid points for LST. N_e = 18 ensemble members, producing a $[N_e \times N_t \times N_p]$ matrix, which is reshaped to $[N_e \times N_t * N_p]$ for generality. However, training a surrogate model for each point in space-time $(N_t * N_p)$ is computationally costly, so we first apply a dimensionality reduction of the problem using Karhunen-Loève expansions (KLE). Using this decomposition, the QoI approximation can be written as,

$$Z = f(\boldsymbol{\lambda}, \boldsymbol{x}, t) \approx \overline{f}(\boldsymbol{x}, t) + \sum_{j=1}^{L} \xi_j(\boldsymbol{\lambda}) \sqrt{\mu_j} \phi_j(\boldsymbol{x}, t) \qquad (2)$$

in terms of uncorrelated, zero-mean, unit-variance random variables $\xi_j(\boldsymbol{\lambda})$ and eigenvalue-eigenfunction pairs $(\mu_j, \phi_j(\boldsymbol{x}, t))$ of the covariance, truncated at eigenvalue L that explains a user-defined level of variance. $\overline{f}(\boldsymbol{x}, t)$ indicates the ensemble mean. In the current problem, we truncate to $L = N_d$ modes of variation that require surrogate approximation. This explains 91% and 93% variance for LST and T2m training sets, respectively. Truncating here produces inverse KLE transform errors of similar magnitude between the training and test sets, limiting overfitting to the training set.

We make a prediction for all the eigenmodes using a single NN surrogate model, minimizing the Huber loss. We use two hidden layers with 15 neurons in each, which is the midpoint between the size of the input layer (=20 after one hot encoding) and the output layer ($L = 9$). A small dropout level (=0.001), is used to reduce overfitting to the small training set (a higher dropout level produces surrogates with unreasonably high joint effect sensitivity indices). The process above is repeated 9 times with different random seeds (111, 222, ..., 999) to provide an uncertainty range for surrogate prediction that can be incorporated into the uncertainty analysis.

The surrogate approximations in KLE space can be converted back to space-time dimensions through the inverse KLE transform. As the full space-time dimension is very large, for our analysis we manipulate $\phi_j(\boldsymbol{x}, t)$ and $\overline{f}(\boldsymbol{x}, t)$ for a subset of interest such as by averaging these functions across $\boldsymbol{x}$ and/or t, and by selecting a subset of $\boldsymbol{x}$ corresponding to a specific lake or area of land. By averaging across both $\boldsymbol{x}$ and t, we get the spatiotemporal average for a set of input parametric priors, $\overline{f}(\boldsymbol{\lambda})$, and use this to summarize the surrogate model errors (Figure 2). From this summary perspective, the surrogate model is able to provide an acceptable prediction for the test set members except for a notable outlier with a very high LST.
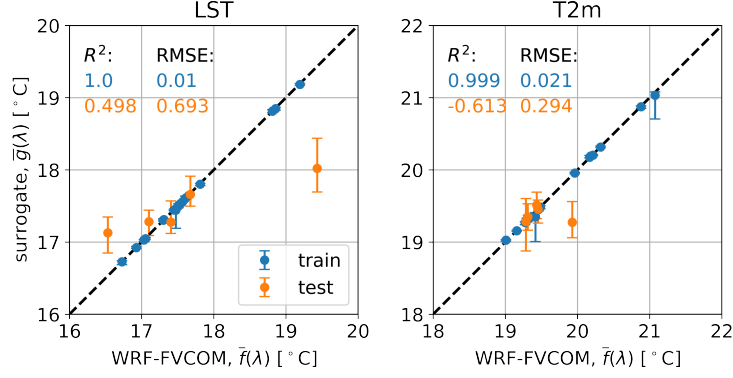
Figure 2. Accuracy of surrogate model predictions of the spatiotemporally-averaged LST and T2m for the training set (N_e=18) and test set (N_{et}=5) with error bars showing the mean and range across the 9 random seeds.
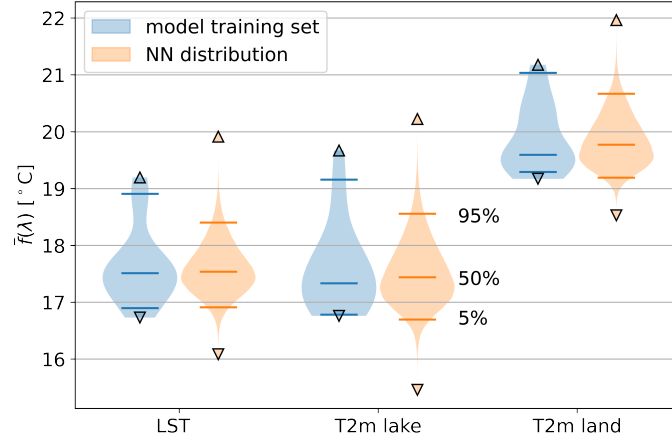

Figure 3. Comparison of the distribution of the spatiotemporally-averaged LST and T2m over the lake and land surface, $\overline{f}(\boldsymbol{\lambda})$, between the surrogate model and the physical model training set. Surrogate model distribution is the concatenation across the 9 random seeds. Triangle markers indicate maximum/minimum values.

3 Results

3.1 Overall

The overall physics uncertainties are estimated as 1.49°C, 1.87°C and 1.48°C for LST, T2m over lake, and T2m over land, respectively, in terms of the 90% interval of $\overline{f}(\boldsymbol{\lambda})$ according to the surrogate model (Figure 3). This highlights the important role that the Great Lakes play on the atmosphere by contributing to greater uncertainty of T2m over the lakes even though the average air temperature over lakes is smaller. Comparing to the distribution of the training set, we find that the 90% interval is reduced in the surrogate model, mostly as a result of a reduction in the 95th percentile value. On the other hand, the surrogate model produces a wider absolute range (maximum minus minimum) and is especially less constrained at the low end of the distribution than the training set.
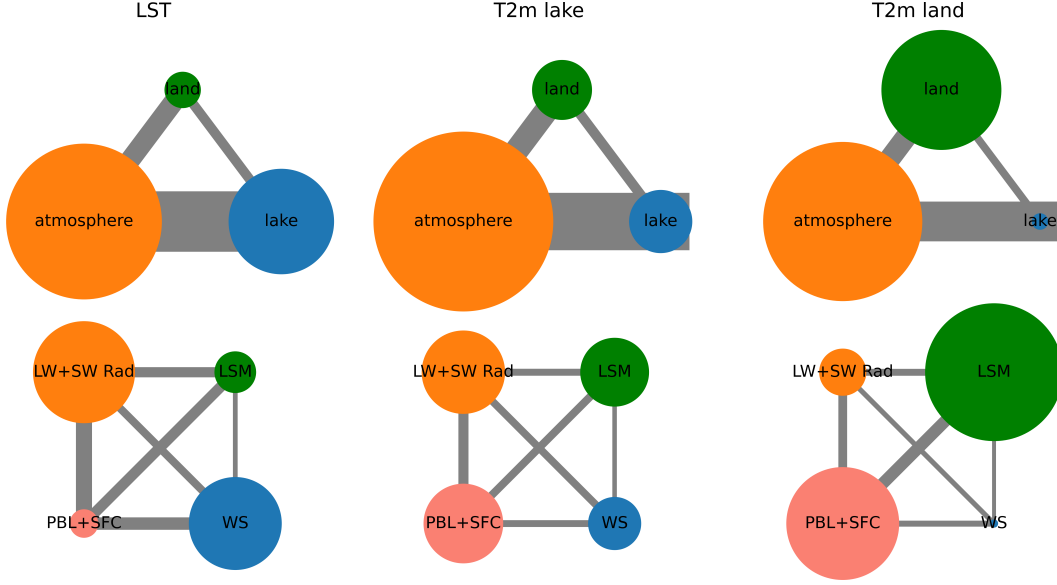
Figure 4. Relative importance of parameterizations/parameters and their interactions to LST and T2m over the lake and land according to the surrogate model. Top: Combined atmosphere, land, and lake parameterizations/parameters. Bottom: Top four important parameterizations (refer Figure 5). The radius of circle corresponds to main effect sensitivity while line thickness corresponds to joint effect sensitivity (same scaling).

A plurality of the physics uncertainty is driven by parameterizations in the atmosphere for both LST and T2m (Figure 4). Depending on the QoI, the impact of lake and land physics and the three-way interactions are also important. LST is particularly sensitive to lake physics while land physics have a small effect; and vice versa for T2m over land. For T2m over lake we find that the relative importance of the land and the lake are similar. Interestingly, however, atmosphere-lake physics interactions are shown to be more important than atmosphere-land and land-lake interactions across all QoIs. For example, although the main effect of lake physics on T2m over land is very small, the importance of the atmosphere-lake interactions is quite substantial and of similar magnitude to the main effect from the land.

For both LST and T2m, we find that the four most significant parameterizations are LW+SW Rad, PBL+SFC, LSM, and WS (Figures 4 and 5). This makes physical sense, as the radiative heat fluxes are the main energy source, and the other parameterizations control how the heat is distributed at the surface. LSM is totally representative of the land contribution, and WS is mostly representative of the total lake contribution. While the importance of atmospheric physics is similar across the QoIs, the contribution from LW+SW Rad and PBL+SFC schemes changes. For LST, the LW+SW Rad is dominant and the effect of PBL + SFC is small, since WS is more important for control of the lake surface. Here, both LW+SW Rad and WS account for 30-40% of the total variance. The opposite is true for T2m over land where the LSM and PBL+SFC scheme dominate, accounting for approximately 40% and 50% of the total variance, respectively. This also makes physical sense as T2m is a quantity interpolated between skin temperature and the lowest atmospheric layer, which are both modulated by LSM and PBL+SFC. While for T2m over lake, the PBL+SFC and LW+SW Rad schemes have comparable impacts of around 30% explained variance. Here, WS explains just below 20% of the variance and LSM explains just above 20%.
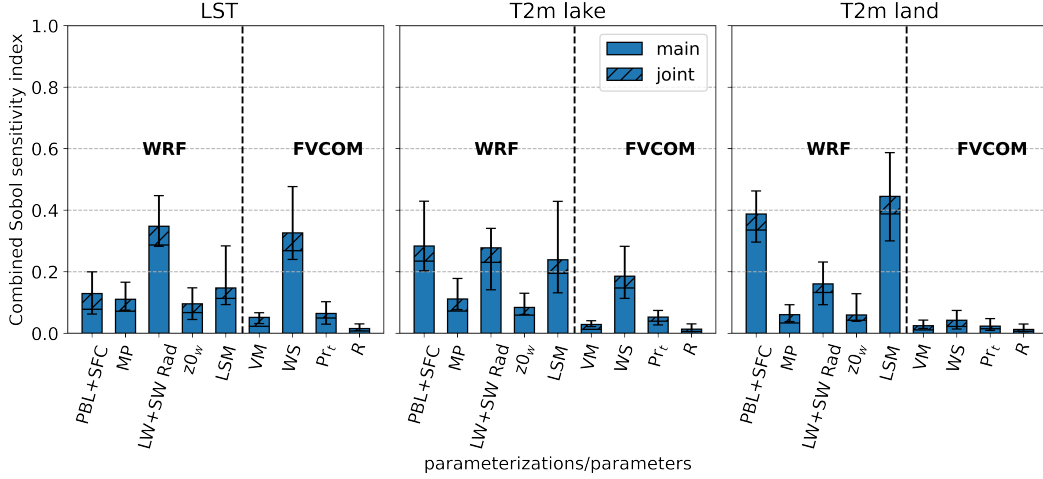
Figure 5. Relative importance (contributions to the total variance, split into main and joint effect Sobol sensitivity components) of all WRF and FVCOM parameterizations/parameters (see Table 1 for explanations) to LST and T2m over the lake and land according to the surrogate model. Error bars show the range across the 9 random seeds.

The most important joint effect sensitivities for LST are between LW+SW Rad, PBL+SFC and WS as these interactions control the available heat flux into the lake. The same is mostly true for T2m over lake, but the joint effect sensitivity between LW+SW Rad and WS is reduced. For T2m over land, the interaction between LSM and PBL+SFC becomes the most significant joint effect sensitivity. The other WRF schemes, PBL+SFC, MP, $z0_w$ and the LSM all have similar magnitudes of sensitivity that explain between 10 and 20% of the variance. Much of this is composed of joint effect sensitivity (except for LSM), meaning a large part of that uncertainty arises from their interactions across different combinations because the coupling does not directly involve the output from these physical parameterizations.

3.2 Spatial Variations

The uncertainty of LST is shown to be largest in the deeper central areas of Lake Superior (Figure 6). Indeed, the uncertainty tends to correlate with the size of the lake, with Lakes Erie and Ontario having the smallest uncertainty on average. This emphasizes the importance of being able to realistically model large and deep lakes with a 3-D hydrodynamic model such as that used in this study.

The higher uncertainty of LST over central Lake Superior is not attributable to any one particular parameterization, but the sensitivity from most of the parameterizations are somewhat elevated here (Figure 7). In general, though, offshore regions are more sensitive to radiation while coastal regions in the northern larger lakes are more sensitive to the lake WS parameterization. This could be explained by the cyclonic summer circulation patterns of the lakes, where currents are generally faster along coastal areas than offshore (Bai et al., 2013). The PBL+SFC scheme is shown to produce higher sensitivity values in specific shallow areas of lakes such as western Lake Erie and the western tip of Lake Huron, where current speeds are very low (Bai et al., 2013). Southeast Lake Michigan is the one area particularly sensitive to the LSM. Although not particularly important, the effect of $z0_w$ is most significant in the shallower southern lakes, which matches the increase in surface roughness as the lake depth decreases for the depth-dependent scheme.
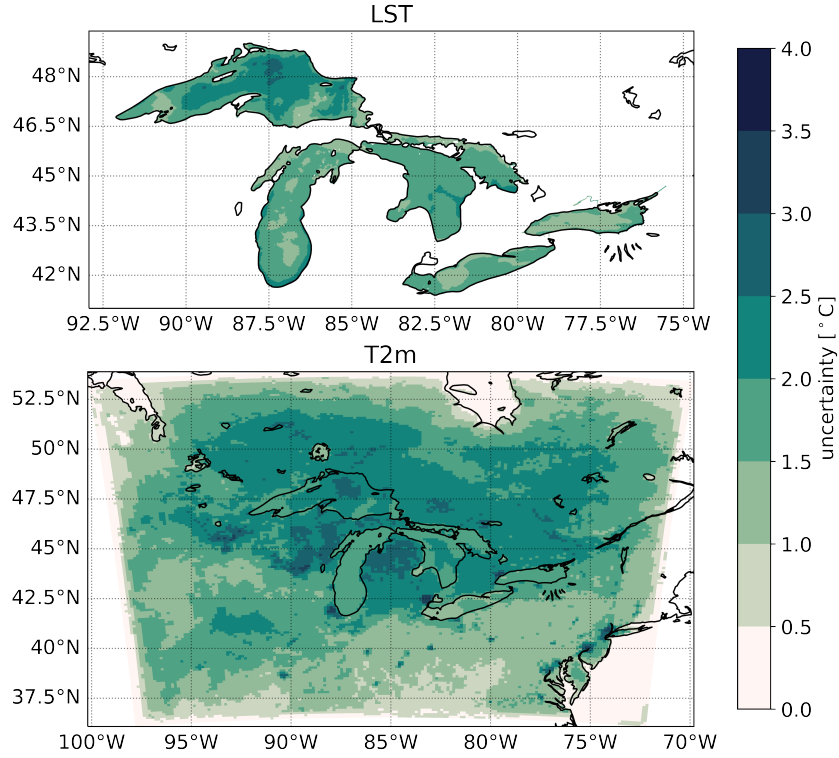
Figure 6. Spatial distribution of LST and T2m physics uncertainty, defined as the 90% interval of the time-averaged surrogate model distribution.
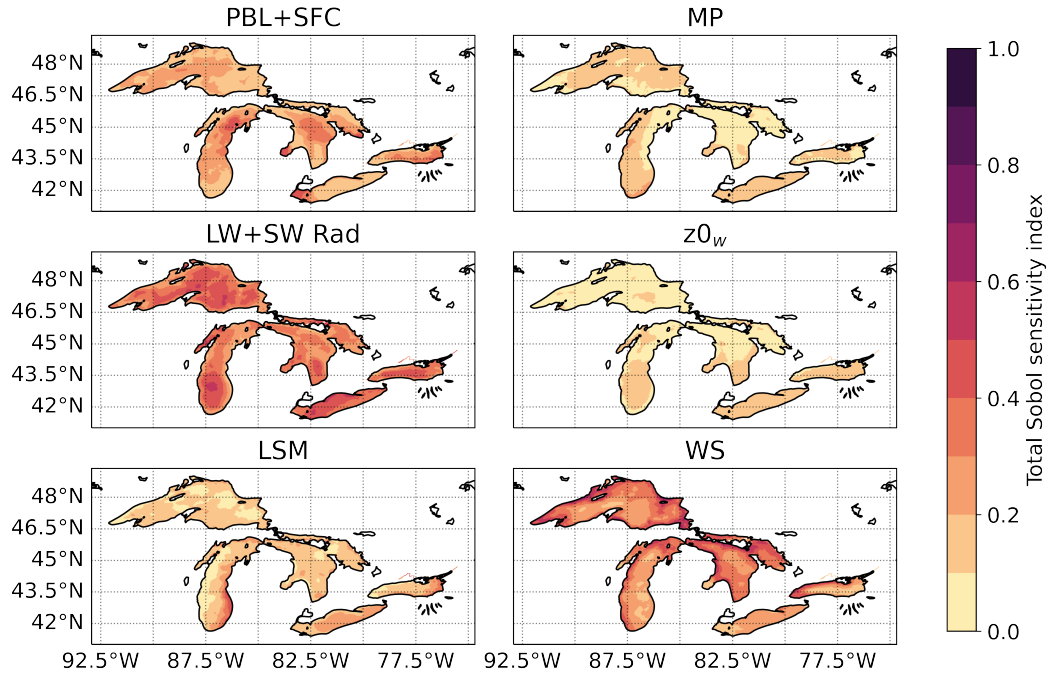

Figure 7. Spatial variation of LST total effect Sobol sensitivity indices for the six most important physics parameterizations (refer Figure 5) according to the time-averaged surrogate model.
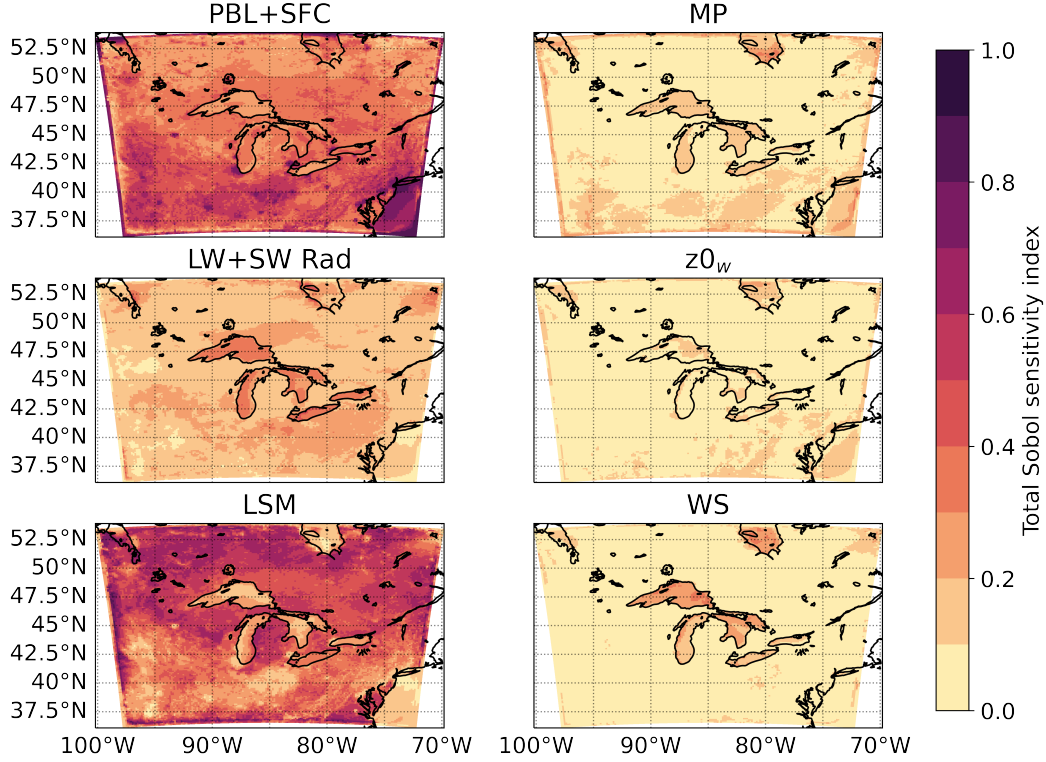
Figure 8. Spatial variation of T2m total effect Sobol sensitivity indices for the six most important physics parameterizations (refer Figure 5) according to the time-averaged surrogate model.

The spatial map shows that T2m uncertainty is highest over land near the northern Great Lakes, over central Lake Superior and in urban areas (Figure 6). The uncertainty of T2m is lowest over land in the southern half of the domain, which explains why the uncertainty of T2m over land is found to be generally lower than over lake (Figure 5). There is a strong correlation between the uncertainty of T2m and LST over Lake Superior (i.e., lower uncertainty in the eastern and western potions of Lake Superior and high uncertainty in the deep central area). T2m is especially uncertain to the west and east of central Lake Michigan and over Chicago and Detroit, which are the largest urban areas in the domain.

For T2m, we see that the radiation and lake WS parameterizations are the most important over the lakes, in agreement with LST (Figure 8). The LSM dominates T2m sensitivity over land around the Great Lakes and to the north where there is a high density of forested area. Noah-MP LSM incorporates several relevant augmentations to Noah, such as a separate vegetation canopy layer with canopy gaps that could produce this effect (Niu et al., 2011). On the other hand, the land around the southern lakes and further south is mainly agricultural, in which differences between the LSMs are small. PBL+SFC is dominant in the south and over urban areas. This makes physical sense due to the southwesterly prevailing winds in the summer (Bai et al., 2013) that the PBL+SFC scheme can have an impact on. Further, urban areas like Chicago are very sensitive to treatment at the surface and can be improved by coupling to an urban canopy model (J. Wang, Qian, et al., 2023).
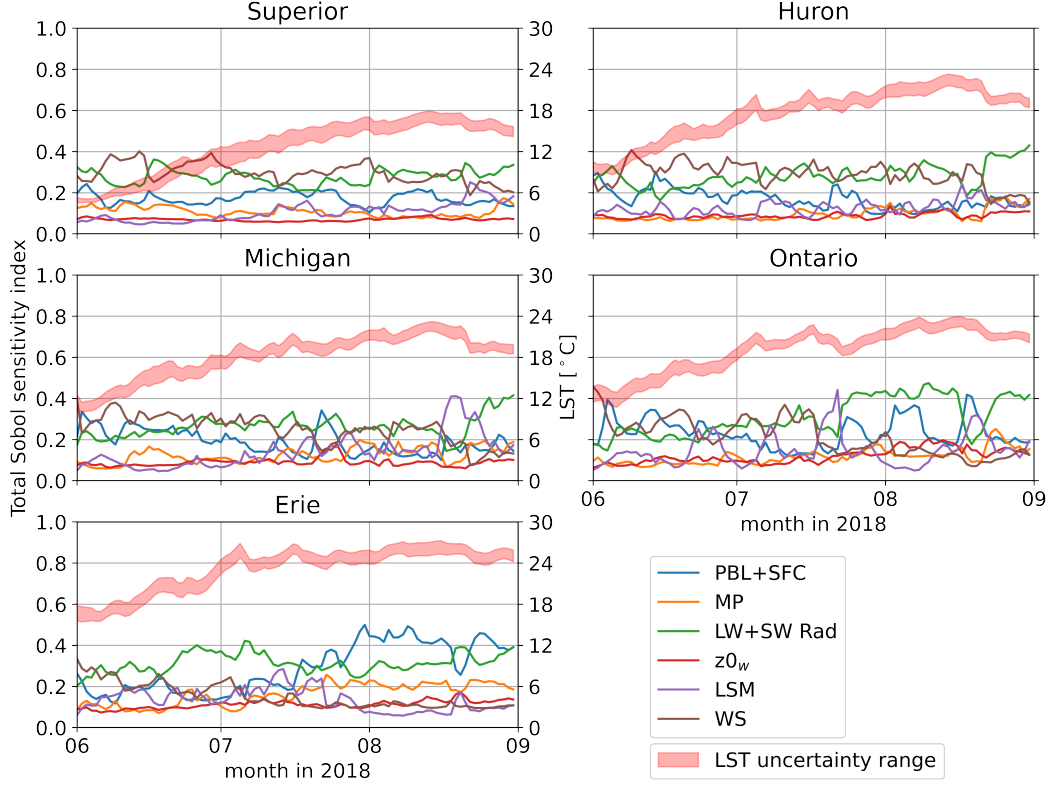
Figure 9. Temporal variation of LST physics uncertainty (the range of the shaded area between the 5th and 95th percentiles) and total effect Sobol sensitivity indices for the six most important parameterizations (refer Figure 5) according to the spatially-averaged surrogate model across each of the five Great Lakes (refer Figure 1).

3.3 Temporal Variations

The uncertainty of LST is shown to be fairly consistent across time for each of the lakes during the summer months studied here (Figure 9). Slightly higher uncertainty is present during the rapid warming phase, which occurs in late June-July for Lake Superior and in June (and earlier) for the other lakes. Lake Superior is shown to have the highest LST uncertainty on average ($1.77\pm0.52°$C) while Lake Ontario has the lowest ($1.51\pm0.31°$C). The high uncertainty in the rapid spring warming phase coincides with elevated sensitivity to WS across all the lakes, highlighting how parameterization of momentum flux at the surface affects the way excess heat entering the lake during that period is distributed. The importance of WS also seems to correlate with lake size or latitude, with Lake Superior and Huron showing the highest sensitivity to WS. The magnitudes of sensitivity across the different parameterizations are more equal in Lake Michigan and Ontario than in the other lakes. They are also the two lakes where we see the largest spikes in LSM sensitivity, in mid-July and mid-August, which may be focused on their east coasts according to Figure 8. It is unclear why this occurs, but both times correspond to a sustained drop in LST.

The LST uncertainty tends to decrease with average lake latitude. This trend is bucked by Lake Erie, which has the second highest LST uncertainty on average ($1.70\pm0.20°$C). Erie is easily the shallowest lake and can therefore be most directly impacted by atmospheric radiation, as shown by an elevated total effect sensitivity index especially dur-
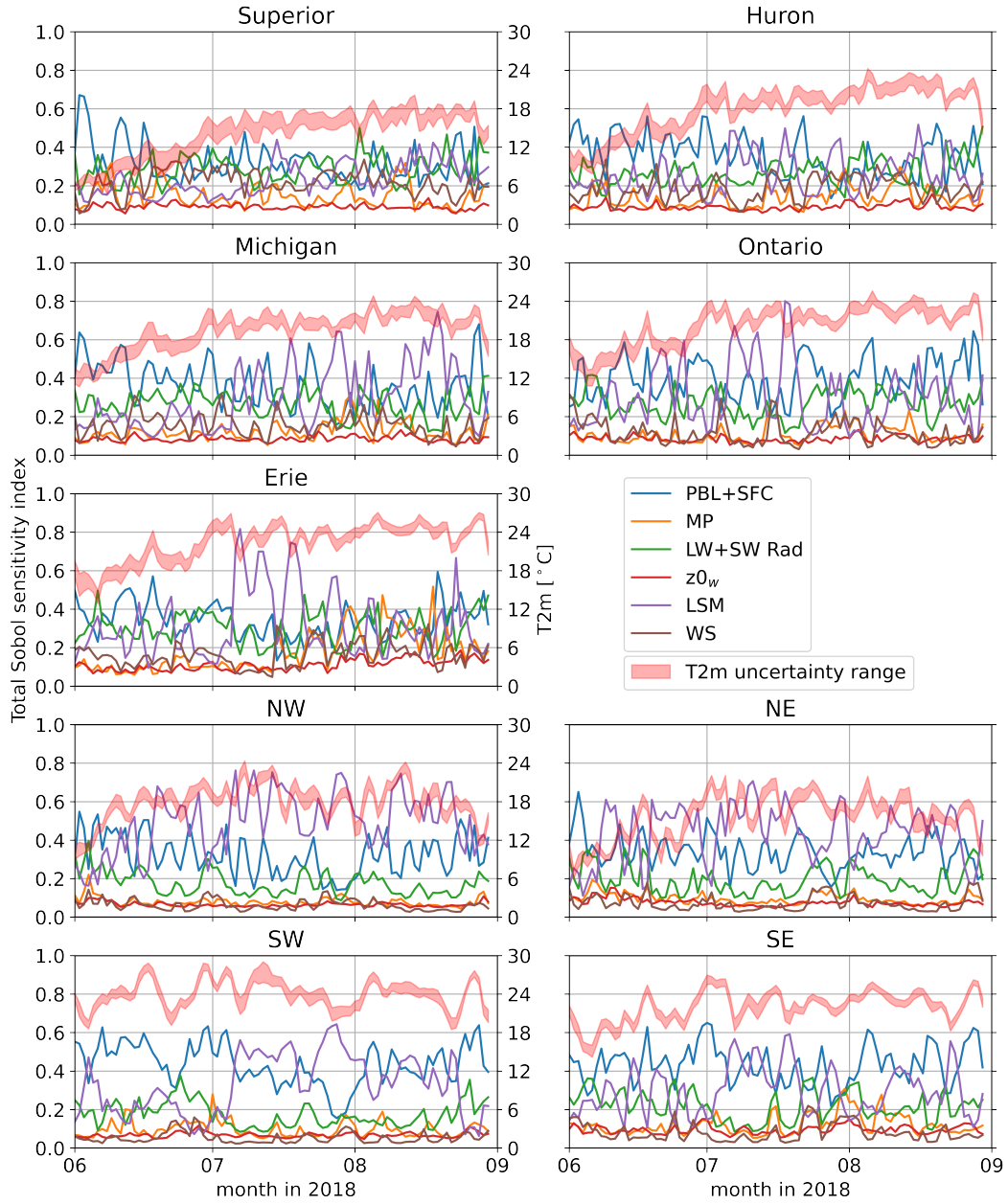
Figure 10. Temporal variation of T2m physics uncertainty (the range of the shaded area between the 5th and 95th percentiles) and total effect Sobol sensitivity indices for the six most important parameterizations (refer Figure 5) according to the spatially-averaged surrogate model across each of the five Great Lakes and the four land quadrants (refer Figure 1).

ing the rapid spring warming phase. Similarly, Erie is less sensitive to WS than the other lakes. The effect of the PBL+SFC scheme from late July-August in Erie is far higher than seen for the other lakes. Spatial plots show this sensitivity is strongest over the extremely shallow western Lake Erie (Figure 7). This influence could be coming from the nearby Detroit urban area and/or northern Indiana to the southwest that has a high sensitivity to PBL+SFC.

The uncertainty of T2m over the lakes is consistent with LST in that higher uncertainty is present during the rapid spring warming phase and correlates with higher latitude lakes (Figure 10). Indeed, Lake Superior has the highest average T2m uncertainty (2.39±0.53°C) while Lake Erie has the lowest (1.77±0.52°C). This latter fact is different from LST where Erie had the second highest average uncertainty. The higher T2m uncertainty in the rapid warming phase is associated with elevated sensitivity to the PBL+SFC scheme. Later in the season, starting from July, the importance of the LSM increases, particularly in the southern lakes. The impact of the radiation parameterization is fairly consistent across the lakes and throughout the season.

Over land, T2m is shown to warm up in June in the northern areas before maintaining a fairly constant temperature until late August. While in the southern areas, T2m maintains a more elevated temperature throughout the season. The average uncertainty of T2m in the northern land areas (NW = 1.80±0.40°C, NE = 1.76±0.45°C) is higher than in the southern areas (SW = 1.60±0.41°C, SE = 1.37±0.34°C), and also higher in the west than in the east. We mostly find that the uncertainty of T2m over land has no clear time variation like over the lakes, except for the SW area, where the uncertainty is significantly larger between early July and mid-August. The uncertainty of T2m over land is mostly being driven by the LSM and PBL+SFC as also shown clearly in Figure 8. The sensitivity to PBL+SFC is consistent throughout the season for the four land areas. In contrast, sensitivity to LSM is more variable with time, especially in the southern areas. The magnitude of this sensitivity increases during July and into August, the same time as the higher uncertainty in the SW. As noted previously, this is correlated with a reduction in temperature over multiple days, and could be related to different runoff and surface soil thermal conductivity treatments in the LSMs (Niu et al., 2011).

4 Discussion and Conclusions

In this study, we presented a surrogate-based approach to evaluate the physics uncertainty in a coupled lake-atmosphere-land model of the GLR. We assessed surface air and lake temperatures using a NN surrogate model that can be rapidly queried to obtain sensitivity and uncertainty information. The sensitivity information from the surrogate model agrees with physical intuition such as producing logical ranking of the relative importance of atmosphere, lake, and land contributions to LST and T2m over lake and land, and describing how atmospheric radiation and lake surface wind stress is the dominant control on LST. This indicates that the surrogate model applied here is robust and physically reasonable for understanding the uncertainties. The MLP-based NN model may be further improved by using other NN types well-suited to time series analysis such as Long Short-Term Memory (Kratzert et al., 2019).

We showed that the physics uncertainty in T2m is on average greater over the lakes than over land, although the uncertainty for T2m over land in the vicinity of the Great Lakes is highest overall. The uncertainty of both LST and T2m tends to be higher in the northern lakes and land areas than in the south. One exception to this rule is that Lake Erie LST is the second most uncertain after Lake Superior, although this higher level of uncertainty arises from different physics (PBL+SFC for Erie and WS for Superior). In regards to temporal variations, uncertainty is highest during the rapid spring warming phase for LST and T2m over the lakes, while T2m over the SW land area is higher between early-July and mid-August.

The primary source of this uncertainty for surface temperatures arises from parameterizations in the atmosphere (mostly LW+SW Rad and PBL+SFC) and a significant contribution from the overall atmosphere-lake physics interaction. The land's LSM and the lake's WS scheme are also critical for T2m and LST, respectively. As expected, LW+SW Rad is important as it controls the heat available to the surface for heating, and there is relatively little spatial and temporal variation of this sensitivity. The other parame-

terizations are all related to surface fluxes in each of the atmosphere, lake, and land model components. Naturally, we find that WS is important for surface temperatures over the lake and unimportant over land, consistent with J. Wang et al. (2022), who found that LST affects air temperature mainly locally. This sensitivity to WS is most pronounced during the rapid spring warming phase and for the larger northern lakes. The effect of PBL+SFC is important especially to the T2m over land in the southern areas, and to LST over Lake Erie, perhaps related to the southwesterly prevailing summer winds. PBL+SFC has the highest sensitivity to T2m over urban areas which can be improved by coupling to an urban canopy model (J. Wang, Qian, et al., 2023). The effect of LSM is, in general, greatest on T2m over the northern land areas, which is more forested than the agricultural south. This makes sense based on the several canopy-based augmentations of the Noah-MP LSM. The temperatures in the southern lakes and land areas also become more sensitive to LSM from early-July to mid-August, coinciding with sustained multiday temperature declines.

One hypothesis of this study was that the $z0_w$ scheme would be important for the Great Lakes as they are much shallower than the open ocean, and the depth-dependent scheme was shown to be important over the shallower continental shelves (Jiménez & Dudhia, 2018). We see here that, at least for surface temperature, the effect of $z0_w$ is relatively minor. However, this could be at least partially because the momentum flux on the atmosphere side and the lake side are calculated independently. If we instead transfer the fluxes computed in WRF (which uses $z0_w$) to FVCOM directly instead of state variables, we should see $z0_w$ assume the higher sensitivity of the WS scheme. We therefore recommend exploring this type of consistent flux-exchange coupling in future iterations of the coupled WRF-FVCOM model.

Other physics of the lake – the attenuation of the shortwave radiation, the vertical mixing scheme and the turbulent Prandtl number – were shown to be relatively unimportant to both lake and atmospheric (near-)surface temperatures. Therefore, careful treatment of atmospheric radiation and surface fluxes, as well as the numerical scheme (J. Wang, Fujisaki-Manome, et al., 2023), should be the focus of further attention in the development and assessment of the coupled WRF-FVCOM model (Kayastha et al., 2023) or similar coupled modeling systems of the GLR (e.g., Sun et al., 2020; Xue et al., 2022). Additionally, other parameterizations should become more important for different QoIs that we intend to look at in future work, such as microphysics (MP) for precipitation (Qian et al., 2015), among others. We also aim to extend the current framework to parametric calibration using observations (e.g., Lu, Ricciuto, Stoyanov, & Gu, 2018; Xu et al., 2022) in a subsequent study.

Finally, what about the magnitude of climate projections in the GLR compared to our estimates of physics uncertainty? We have recently conducted Pseudo-Global Warming experiments using projections of T2m from the Coupled Model Intercomparison Project Phase 6 (CMIP6) in the GLR under the Shared Socioeconomic Pathway 5 (SSP-8.5) (Yang et al., 2024; Kayastha et al., 2024). An ensemble mean across 12 global climate models shows an increase of 3-5°C by mid-century above 1981-2010 levels (Figure 11). In another study using CMIP5 models, a more modest increase of 1.3-2.1°C by mid-century under the Representative Concentration Pathway (RCP) 8.5 scenario is projected, but this is above 2000-2019 levels (Xue et al., 2022). Our physics uncertainties for T2m average to around 1.5-1.9°C, and based on these numbers would be considered comparable to the Xue et al. (2022) climate change signal, but well below our CMIP6 signal. However, this 90% uncertainty range is two-sided and therefore overstates the close proximity to one-sided projections of (only) warmer temperatures. In fact, we can show that T2m warming need only exceed at most 0.5°C to be statistically greater than physics uncertainty (Figure 11). This estimate was calculated using a Mann-Whitney U test between the surrogate model anomaly distribution and the CMIP6 climate projection ensemble reduced by a spatially varying factor. The sort after result is the minimum warm-
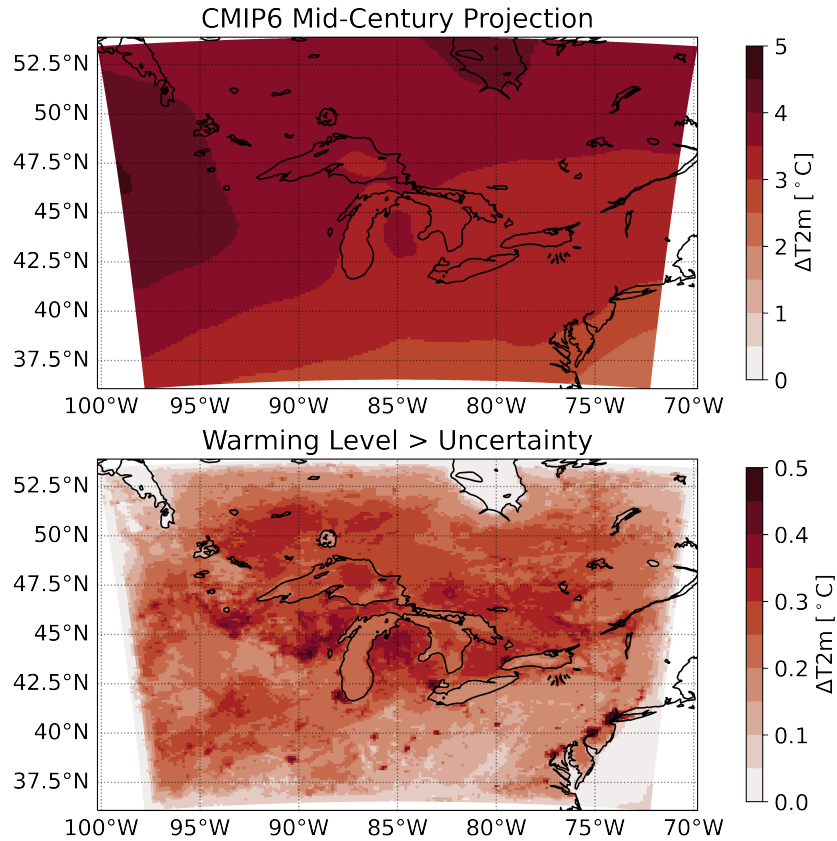
Figure 11. Top: CMIP6 ensemble mean projections of increases in T2m by mid-century (2031–2060) compared to 1981–2010 under the SSP-8.5 scenario. Bottom: T2m warming required to be statistically greater than the physics uncertainty.

ing where we can reject the null hypothesis with $p < 0.05$ in favor of the alternate that warming is greater than physics uncertainty. Of course, other uncertainties exist (Hawkins & Sutton, 2009), such as those that come from initial and boundary conditions or land use/land cover change and SSP scenarios, and these should be incorporated in future work.

5 Open Research

The metarepository for this study is available from `https://github.com/COMPASS-DOE/GreatLakes_CoupledModel_Uncertainty` (W. Pringle, 2024). It contains the uncertainty analysis codes and figures and links to source codes and processed data.

References

Andreas, E. L., Mahrt, L., & Vickers, D. (2012). A new drag relation for aerodynamically rough flow over the ocean. *Journal of the Atmospheric Sciences*, *69*(8), 2520–2537. doi: 10.1175/JAS-D-11-0312.1

Austin, J. A. (2019). Observations of radiatively driven convection in a deep lake. *Limnology and Oceanography*, *64*(5), 2152–2160. doi: 10.1002/lno.11175

Bai, X., Wang, J., Schwab, D. J., Yang, Y., Luo, L., Leshkevich, G. A., & Liu, S. (2013). Modeling 1993-2008 climatology of seasonal general circulation and thermal structure in the Great Lakes using FVCOM. *Ocean Modelling*, *65*, 40–63. Retrieved from http://dx.doi.org/10.1016/j.ocemod.2013.02.003 doi: 10.1016/j.ocemod.2013.02.003

Bellprat, O., Kotlarski, S., Lüthi, D., & Schär, C. (2012a). Exploring perturbed physics ensembles in a regional climate model. *Journal of Climate*, *25*(13), 4582–4599. doi: 10.1175/JCLI-D-11-00275.1

Bellprat, O., Kotlarski, S., Lüthi, D., & Schär, C. (2012b). Objective calibration of regional climate models. *Journal of Geophysical Research Atmospheres*, *117*(23), 1–13. doi: 10.1029/2012JD018262

Briley, L. J., Rood, R. B., & Notaro, M. (2021). Large lakes in climate models: A Great Lakes case study on the usability of CMIP5. *Journal of Great Lakes Research*, *47*(2), 405–418. Retrieved from https://doi.org/10.1016/j.jglr.2021.01.010 doi: 10.1016/j.jglr.2021.01.010

Chen, C., Beardsley, R. C., Cowles, G., Qi, J., Lai, Z., Gao, G., ... Lin, H. (2011). *An Unstructured-Grid, Finite-Volume Community Ocean Model: FVCOM User Manual (3rd edition)*. Retrieved from http://fvcom.smast.umassd.edu/wp-content/uploads/2013/11/MITSG{_}12-25.pdf

Chen, C., Liu, H., & Beardsley, R. C. (2003). An unstructured grid, finite-volume, three-dimensional, primitive equations ocean model: Application to coastal ocean and estuaries. *Journal of Atmospheric and Oceanic Technology*, *20*(1), 159–186. doi: 10.1175/1520-0426(2003)020⟨0159:AUGFVT⟩2.0.CO;2

Craig, A., Valcke, S., & Coquart, L. (2017). Development and performance of a new version of the OASIS coupler, OASIS3-MCT-3.0. *Geoscientific Model Development*, *10*(9), 3297–3308. doi: 10.5194/gmd-10-3297-2017

Edson, J. B., Jampana, V., Weller, R. A., Bigorre, S. P., Plueddemann, A. J., Fairall, C. W., ... Hersbach, H. (2013). On the exchange of momentum over the open ocean. *Journal of Physical Oceanography*, *43*(8), 1589–1610. doi: 10.1175/JPO-D-12-0173.1

Eidhammer, T., Gettelman, A., Thayer-Calder, K., Watson-Parris, D., Elsaesser, G., Morrison, H., ... Mccoy, D. (2024). An Extensible Perturbed Parameter Ensemble (PPE) for the Community Atmosphere Model Version 6. *EGUsphere*, [preprint].

Fang, K.-T., Lin, D. K. J., Winker, P., & Zhang, Y. (2000, aug). Uniform Design: Theory and Application. *Technometrics*, *42*(3), 237–248. Retrieved from https://www.tandfonline.com/doi/abs/10.1080/00401706.2000.10486045 doi: 10.1080/00401706.2000.10486045

Hawkins, E., & Sutton, R. (2009). The potential to narrow uncertainty in regional climate predictions. *Bulletin of the American Meteorological Society*, *90*(8), 1095–1107. doi: 10.1175/2009BAMS2607.1

Hersbach, H., Bell, B., Berrisford, P., Hirahara, S., Horányi, A., Muñoz-Sabater, J., ... Thépaut, J. N. (2020). The ERA5 global reanalysis. *Quarterly Journal of the Royal Meteorological Society*, *146*(730), 1999–2049. doi: 10.1002/qj.3803

Huber, M. B., & Zanna, L. (2017). Drivers of uncertainty in simulated ocean circulation and heat uptake. *Geophysical Research Letters*, *44*(3), 1402–1413. doi: 10.1002/2016GL071587

Jiménez, P. A., & Dudhia, J. (2018). On the need to modify the sea surface roughness formulation over shallow waters. *Journal of Applied Meteorology and Climatology*, *57*(5), 1101–1110. doi: 10.1175/JAMC-D-17-0137.1

Kayastha, M. B., Huang, C., Wang, J., Pringle, W. J., Chakraborty, T., Yang, Z., ... Xue, P. (2023). Insights on Simulating Summer Warming of the Great Lakes: Understanding the Behavior of a Newly Developed Coupled Lake-Atmosphere Modeling System. *Journal of Advances in Modeling Earth Systems*, *15*, e2023MS003620. doi: 10.1029/2023MS003620

Kayastha, M. B., Huang, C., Wang, J., Yang, Z., Pringle, W. J., Chakraborty, T., ... Xue, P. (2024). How will Future Climate Reshape Devastating Lake-Effect Snow Storms? *Nature Communications*, submitted.

Kratzert, F., Klotz, D., Shalev, G., Klambauer, G., Hochreiter, S., & Nearing, G. (2019). Towards learning universal, regional, and local hydrological behaviors via machine learning applied to large-sample datasets. *Hydrology and Earth System Sciences*, *23*(12), 5089–5110. doi: 10.5194/hess-23-5089-2019

Large, W. G., & Pond, S. (1981). Open Ocean Momentum Flux Measurements in Moderate to Strong Winds. *Journal of Physical Oceanography*, *11*, 324–336. doi: 10.1175/1520-0485(1981)011⟨0324:OOMFMI⟩2.0.CO;2

Lu, D., Ricciuto, D., Stoyanov, M., & Gu, L. (2018). Calibration of the E3SM Land Model Using Surrogate-Based Global Optimization. *Journal of Advances in Modeling Earth Systems*, *10*(6), 1337–1356. doi: 10.1002/2017MS001134

Mellor, G. L., & Yamada, T. (1982). Development of a Turbulence Closure Model for Geophysical Fluid Problems. *Reviews of Geophysics and Space Physics*, *20*(4), 851–875. doi: 10.1029/RG020i004p00851

Niu, G. Y., Yang, Z. L., Mitchell, K. E., Chen, F., Ek, M. B., Barlage, M., ... Xia, Y. (2011). The community Noah land surface model with multiparameterization options (Noah-MP): 1. Model description and evaluation with local-scale measurements. *Journal of Geophysical Research Atmospheres*, *116*(12), 1–19. doi: 10.1029/2010JD015139

Notaro, M., Zhong, Y., Xue, P., Peters-Lidard, C., Cruz, C., Kemp, E., ... Vavrus, S. J. (2021). Cold Season Performance of the NU-WRF Regional Climate Model in the Great Lakes Region. *Journal of Hydrometeorology*, *22*, 2423–2454. doi: 10.1175/jhm-d-21-0025.1

Paszke, A., Gross, S., Massa, F., Lerer, A., Bradbury, J., Chanan, G., ... Chintala, S. (2019). PyTorch: An Imperative Style, High-Performance Deep Learning Library. In *Advances in neural information processing systems 32* (pp. 8024–8035). Curran Associates, Inc. Retrieved from http://papers.neurips.cc/paper/9015-pytorch-an-imperative-style-high-performance-deep-learning-library.pdf

Paulson, C. A., & Simpson, J. J. (1977). Irradiance Measurements in the Upper Ocean. *Journal of Physical Oceanography*, *7*(6), 952–956. doi: 10.1175/1520-0485(1977)007⟨0952:IMITUO⟩2.0.CO;2

Pringle, W. (2024). *COMPASS-DOE/GreatLakes_CoupledModel_Uncertainty (v0.1)* [Workflow]. Zenodo. doi: 10.5281/zenodo.10806950

Pringle, W. J., Burnett, Z., Sargsyan, K., Moghimi, S., & Myers, E. (2023). Efficient Probabilistic Prediction and Uncertainty Quantification of Tropical Cyclone-driven Storm Tides and Inundation. *Artificial Intelligence for the Earth Systems*, *2*(2), e220040. doi: 10.1175/AIES-D-22-0040.1

Qian, Y., Guo, Z., Larson, V. E., Leung, L. R., Lin, W., Ma, P. L., ... Zhang,

Y. (2024). Region and cloud regime dependence of parametric sensitivity in E3SM atmosphere model. *Climate Dynamics*, *62*(2), 1517–1533. Retrieved from https://doi.org/10.1007/s00382-023-06977-3 doi: 10.1007/s00382-023-06977-3

Qian, Y., Wan, H., Yang, B., Golaz, J. C., Harrop, B., Hou, Z., ... Zhang, K. (2018). Parametric Sensitivity and Uncertainty Quantification in the Version 1 of E3SM Atmosphere Model Based on Short Perturbed Parameter Ensemble Simulations. *Journal of Geophysical Research: Atmospheres*, *123*(23), 13,046–13,073. doi: 10.1029/2018JD028927

Qian, Y., Yan, H., Hou, Z., Johannesson, G., Klein, S. A., Lucas, D., ... Zhao, C. (2015). Parametric sensitivity analysis of precipitation at global and local scales in the Community Atmosphere Model CAM5. *Journal of Advances in Modeling Earth Systems*, *7*, 382–411. doi: 10.1002/2014MS000354

Ricciuto, D., Sargsyan, K., & Thornton, P. (2018). The Impact of Parametric Uncertainties on Biogeochemistry in the E3SM Land Model. *Journal of Advances in Modeling Earth Systems*, *10*(2), 297–319. doi: 10.1002/2017MS000962

Saltelli, A. (2002). Making best use of model evaluations to compute sensitivity indices. *Computer Physics Communications*, *145*(2), 280–297. doi: 10.1016/S0010-4655(02)00280-1

Sargsyan, K., Safta, C., Najm, H. N., Debusschere, B. J., Ricciuto, D., & Thornton, P. (2014). Dimensionality reduction for complex models via Bayesian compressive sensing. *International Journal for Uncertainty Quantification*, *4*(1), 63–93. doi: 10.1615/Int.J.UncertaintyQuantification.2013006821

Sharma, A., Hamlet, A. F., Fernando, H. J., Catlett, C. E., Horton, D. E., Kotamarthi, V. R., ... Wuebbles, D. J. (2018). The Need for an Integrated Land-Lake-Atmosphere Modeling System, Exemplified by North America's Great Lakes Region. *Earth's Future*, *6*(10), 1366–1379. doi: 10.1029/2018EF000870

Skamarock, W. C., & Klemp, J. B. (2008). A time-split nonhydrostatic atmospheric model for weather research and forecasting applications. *Journal of Computational Physics*, *227*(7), 3465–3485. doi: 10.1016/j.jcp.2007.01.037

Skamarock, W. C., Klemp, J. B., Dudhia, J., Gill, D. O., Liu, Z., Berner, J., ... Huang, X.-Y. (2021). *A Description of the Advanced Research WRF Model Version 4.3* (Vols. TN–556+STR; Tech. Rep.). doi: 10.5065/1dfh-6p97

Stips, A., Burchard, H., Bolding, K., & Eifler, W. (2002). Modelling of convective turbulence with a two-equation k-ϵ turbulence closure scheme. *Ocean Dynamics*, *52*(4), 153–168. doi: 10.1007/s10236-002-0019-2

Sun, L., Liang, X. Z., & Xia, M. (2020). Developing the Coupled CWRF-FVCOM Modeling System to Understand and Predict Atmosphere-Watershed Interactions Over the Great Lakes Region. *Journal of Advances in Modeling Earth Systems*, *12*(12), e2020MS002319. doi: 10.1029/2020MS002319

Wang, C., Qian, Y., Duan, Q., Huang, M., Yang, Z., Berg, L. K., ... Quan, J. (2021). Quantifying physical parameterization uncertainties associated with land-atmosphere interactions in the WRF model over Amazon. *Atmospheric Research*, *262*, 105761. Retrieved from https://doi.org/10.1016/j.atmosres.2021.105761 doi: 10.1016/j.atmosres.2021.105761

Wang, J., Fujisaki-Manome, A., Kessler, J., Cannon, D., & Chu, P. (2023). Inertial instability and phase error in Euler forward predictor-corrector time integration schemes: Improvement of modeling Great Lakes thermal structure and circulation using FVCOM. *Ocean Dynamics*. Retrieved from https://doi.org/10.1007/s10236-023-01558-8 doi: 10.1007/s10236-023-01558-8

Wang, J., Qian, Y., Pringle, W. J., Chakraborty, T. C., Hetland, R., Yang, Z., & Xue, P. (2023). Contrasting effects of lake breeze and urbanization on heat stress in Chicago metropolitan area. *Urban Climate*, *48*, 101429. Retrieved from https://doi.org/10.1016/j.uclim.2023.101429 doi: 10.1016/j.uclim.2023.101429

Wang, J., Xue, P., Pringle, W. J., Yang, Z., & Qian, Y. (2022). Impacts of Lake Surface Temperature on the Summer Climate Over the Great Lakes Region. *Journal of Geophysical Research: Atmospheres*, *127*(11), e2021JD036231. doi: 10 .1029/2021JD036231

Xu, D., Bisht, G., Sargsyan, K., Liao, C., & Ruby Leung, L. (2022). Using a surrogate-assisted Bayesian framework to calibrate the runoff-generation scheme in the Energy Exascale Earth System Model (E3SM) v1. *Geoscientific Model Development*, *15*(12), 5021–5043. doi: 10.5194/gmd-15-5021-2022

Xue, P., Pal, J. S., Ye, X., Lenters, J. D., Huang, C., & Chu, P. Y. (2017). Improving the simulation of large lakes in regional climate modeling: Two-way lake-atmosphere coupling with a 3D hydrodynamic model of the great lakes. *Journal of Climate*, *30*(5), 1605–1627. doi: 10.1175/JCLI-D-16-0225.1

Xue, P., Ye, X., Pal, J. S., Chu, P. Y., Kayastha, M. B., & Huang, C. (2022). Climate projections over the Great Lakes Region: using two-way coupling of a regional climate model with a 3-D lake model. *Geoscientific Model Development*, *15*(11), 4425–4446. doi: 10.5194/gmd-15-4425-2022

Yang, Z., Wang, J., Qian, Y., Chakraborty, T. C., Xue, P., Pringle, W. J., . . . Hetland, R. (2024). Summer Convective Precipitation Changes over the Great Lakes Region under a Warming Scenario. *Journal of Geophysical Research: Atmospheres*, submitted.

Zanna, L., Brankart, J. M., Huber, M., Leroux, S., Penduff, T., & Williams, P. D. (2019). Uncertainty and scale interactions in ocean ensembles: From seasonal forecasts to multidecadal climate predictions. *Quarterly Journal of the Royal Meteorological Society*, *145*(S1), 160–175. doi: 10.1002/qj.3397